

# Rotational Damping, Ridges And The Quasi-Continuum Of $\gamma$ Rays In $^{152}\text{Dy}$

T. Lauritsen\*, R.V.F. Janssens\*, T.L. Khoo\*, I. Ahmad\*, M.P. Carpenter\*,  
A.M. Heinz\*, D.G. Jenkins\*, F.G. Kondev\*, C.J. Lister\*, E.F. Moore\*,  
D. Seweryniak\*, S. Zhu\*, T. Døssing<sup>†</sup>, B. Herskind<sup>†</sup>, R.M. Clark\*\*, M. Cromaz\*\*,  
P. Fallon\*\*, G. Lane\*\*, A.O. Macchiavelli\*\*, D. Ward\*\*, A. Korichi<sup>‡</sup>,  
A. Lopez-Martens<sup>‡</sup> and A.J. Larabee<sup>§</sup>

\*Physics Division, Argonne National Laboratory, Argonne, Illinois 60439, USA.

<sup>†</sup>Niels Bohr Institute, DK-2100, Copenhagen, Denmark.

\*\*Lawrence Berkeley National Laboratory, Berkeley, California 94720, USA.

<sup>‡</sup>C.S.N.S.M, IN2P3-CNRS, bat 104-108, F-91405 Orsay Campus, France.

<sup>§</sup>Greenville College, Greenville, Illinois 62246, USA.

**Abstract.** Both the quasi-continuum of  $\gamma$  rays as well as the ridges from the feeding (and decay) of superdeformed and normal bands have been extracted in the nucleus  $^{152}\text{Dy}$ . A model has been developed that *simultaneously* describes all these spectra as well as the feeding intensity of the superdeformed bands. Through the calculation of the continuum of  $\gamma$  rays at finite temperature, the rotational damping width in the normal and superdeformed wells are extracted. This is the first time the rotational damping width in a superdeformed well has been measured in the  $A \sim 150$  mass region.

## INTRODUCTION

In a number of nuclei, strong deforming shell effects lead to an excited minimum associated with large, prolate deformation (with a major to minor axis ratio of  $\sim 2:1$ ) [1, 2]. The properties of the excitations occurring in this superdeformed (SD) minimum continue to be a subject of much interest. Superdeformation in  $^{152}\text{Dy}$  was originally discovered by studying ridges, i.e., structures parallel to the diagonal, in  $\gamma - \gamma$  coincidence matrices [3, 4]. Only afterwards was the first discrete SD band discovered [5] in this nucleus. It took 16 years to link this SD band to the normal deformed (ND) states it decays into [6], and recently SD band 6, built on an octupole vibration, was linked to the yrast SD band [7] as well. These two feats were only possible because a *very* large data set was collected with Gammasphere [8]. This data set also makes it possible to take a new look at the quasi-continuum (QC) of  $\gamma$  rays with much higher precision.

In itself it is important to study the QC of  $\gamma$  rays as a means to elucidate the feeding mechanism of SD and ND bands in heavy-ion fusion reactions [9, 10]. Moreover, the QC has been used to determine the spin and energy of SD bands when discrete linking transitions cannot be found [9]. The correlations in the  $\gamma - \gamma$  coincidence matrices furthermore allow for a determination of the important rotational damping [11, 12, 13, 14, 15, 16, 17, 18] at finite temperature. Here the level density may be so high that E2 transitions are no longer just simple intra-band transitions: the initial and final states are complicated superpositions resulting from the mixing of a large number of states. The ensuing distribution of  $\gamma$ -ray energies out of each state acquires a width, the rotational damping width, the FWHM of which is denoted  $\Gamma_{wide}$ . In addition,  $\gamma - \gamma$  correlation matrices also address more specific two step correlations, described by a more narrow width,  $\Gamma_{nar}$  [15, 16, 17, 18]. The main aim of this work is to extract  $\Gamma_{wide}$ ,  $\Gamma_{nar}$  and the relative intensities of the wide and narrow components for  $^{152}\text{Dy}$ .

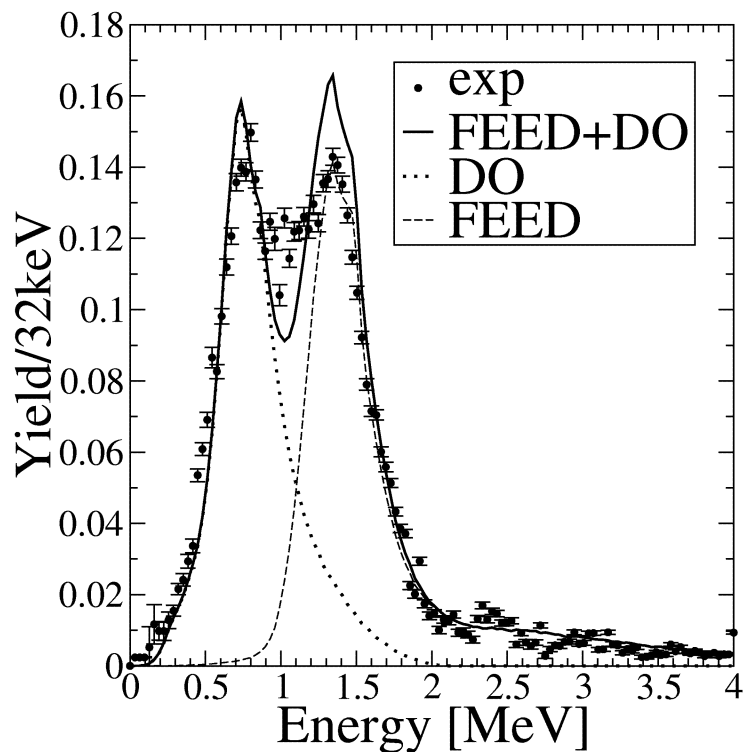


**Figure 1.** The QC of  $\gamma$  rays when double coincidence gates are set on clean combinations of SD lines from band 1 in  $^{152}\text{Dy}$  [6]. The data have been sorted spike free and for the different polar angles of Gammasphere. Local background spectra were subtracted [19] before unfolding [20]. The discrete peaks were removed and the points with error bars are the sum of angle sorted spectra after correction for Doppler shifts. The dotted curve shows the calculation of the decay-out QC (sum of statistical E1 and quadrupole E2 transitions) and the dashed curve is the calculation of the feeding QC. The solid line is the sum of these two calculated QC components.

## EXPERIMENTAL DETAILS

ND and SD bands were populated in  $^{152}\text{Dy}$  using the reaction  $^{108}\text{Pd}(^{48}\text{Ca},4n)^{152}\text{Dy}$  at 194 MeV (mid target). The  $^{48}\text{Ca}$  beam was delivered by the 88 inch cyclotron facility at the Lawrence Berkeley National Laboratory and the target consisted of a stack of two  $\sim 0.4$  mg/cm<sup>2</sup> self-supporting  $^{108}\text{Pd}$  foils. The  $\gamma$  rays were measured with the Gammasphere array [8], comprised of 100 Compton suppressed germanium detectors. As described in Ref. [6], events associated with the  $^{152}\text{Dy}$  reaction channel were tagged by detecting (with an efficiency of  $\sim 80\%$ ) the decay of the 86 ns,  $17^+$  yrast isomer [21], in the most forward BGO detectors [22] of the array. A total of  $1.6 \times 10^9$  events were tagged from the  $^{152}\text{Dy}$  reaction channel.

## THE QUASI-CONTINUUM

Double coincidence gates were placed on clean combinations of transitions in the SD band 1 in  $^{152}\text{Dy}$  [6] and the resulting spectra carefully background subtracted [19] with local background spectra in each Gammasphere polar angle. The spectra were then corrected for neutron interactions [10], unfolded [20] and normalized to the number of  $\gamma$  cascades. The sum of angle sorted spectra, after removal of the discrete peaks, and a correction for Doppler shifts, is shown in Fig. 1. The QC spectrum clearly shows two components: one is from the feeding of the SD band and the other is associated with the decay-out (DO) of the SD band to ND states at lower spins. Fig. 2 shows the QC of  $\gamma$  rays when double coincidence gates are set on normal transitions in  $^{152}\text{Dy}$ . For both spectra an isomer tag was required as well.

## THE RIDGE SPECTRA

Just as the QC spectra were extracted by placing double coincidence gates on ND and SD lines, 2D matrices were generated using the same combination of clean gates. In addition to double-gated matrices, single-gated and un-gated matrices were generated as well so that the double gated matrices could be background subtracted using a modified

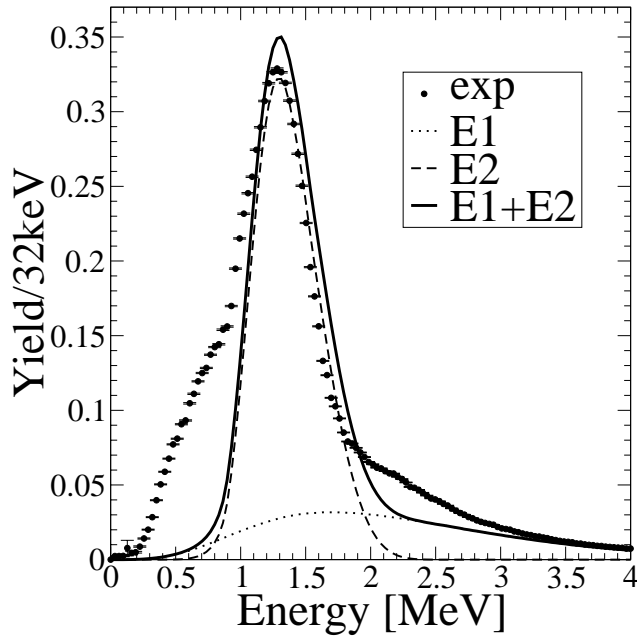


**Figure 2.** The QC of  $\gamma$  rays when double coincidence gates are placed on a combination of ND transitions in the spin range  $28\text{--}37\hbar$  in  $^{152}\text{Dy}$ . The isomer tag is required as well. The spectrum is similar to that reported in [10]. The dotted line is a calculated E1 statistical feeding spectrum, the dashed curve shows the calculated E2 quadrupole  $\gamma$ -ray spectrum and the solid line is the sum of these two calculated components. As in Fig. 1, the model calculation does not yet include the third M1/E2 dipole QC component originating from the last step into the discrete line region at low energy ( $< 1$  MeV).

version of the background subtraction method of Ref. [19], now with matrices instead of 1-dimensional spectra. The background subtracted double gated matrices were unfolded using a 2D version of Radford's unfolding procedure [20]. The matrices were then 'COR subtracted' [23], i.e., an uncorrelated matrix (but only of the relevant local region) is generated from a projection and subtracted so that the resulting matrix has no net counts. The resulting matrix will indicate more than average correlation areas with positive counts (most notably  $\gamma\text{--}\gamma$  peaks and QC coincidences) and under-correlated areas with negative counts (with the area along the diagonal the most obvious example – since  $\gamma$  rays tend not to be in coincidence with  $\gamma$  rays of the same energy).

Before performing a projection of these matrices onto an axis perpendicular to the diagonal, resulting in the so-called 'ridge spectra', it is very important to remove any discrete peaks in the region that is projected. For relatively strong peaks in the matrices, especially in the double SD gated matrix, the entire stripes along the  $E_{\gamma_1}$  and  $E_{\gamma_2}$  axes are removed in order to discard the overwhelming contribution from these 'stripes' to the cross-diagonal projection. In the procedure used in this work, no 'repairs' are made for peaks and stripes removed. Instead, the effect of the missing matrix areas is extracted and used to *correct* the cross-diagonal projections from the matrices with the missing stripes and single correlations. It can be shown that the resulting ridges are very close to the true ridges. The calculated ridges, discussed below, are treated *exactly* in the same way so that any possible artifacts from removing peaks and stripes do not affect the comparison between the experimental data and the simulations. Fig. 3 shows the calculated ND ridges obtained this way and Fig. 4 presents the SD ridges.

## CALCULATIONS

A Monte Carlo approach is used to *simultaneously* reproduce both the QC spectra in Figs. 1 and 2 and the ridges in Figs. 3 and 4. The code also reproduces the  $\sim 2\%$  SD feeding, among other features. The Monte Carlo model used in the mass  $A \sim 190$  region [9] was modified to handle the two components of the damping,  $\Gamma_{wide}$  and  $\Gamma_{nar}$ , which theory [15] suggest should be necessary (as confirmed in this analysis) in order to reproduce the observed ridges in Figs. 3 and 4. The calculation follows the  $\gamma$  cascades from the entry distribution, i.e., the region in the spin and energy plane populated after the last particle has been evaporated. The  $\gamma$  cascades are followed until they are close ( $\sim 1$  MeV) to either the ND or SD yrast lines, when M1/E2  $\gamma$  rays are emitted in the last few steps towards the discrete states of the nucleus [9].

For each step, a total of eight decay widths are calculated: namely those of E2 quadrupole transitions and E1 statistical transitions ( $\Delta I = -1, 0, 1$ ) in both the ND and SD wells. If the nucleus is SD at the time of decay, the four decay widths in the ND well are attenuated by the penetration probability through the barrier that separates the ND

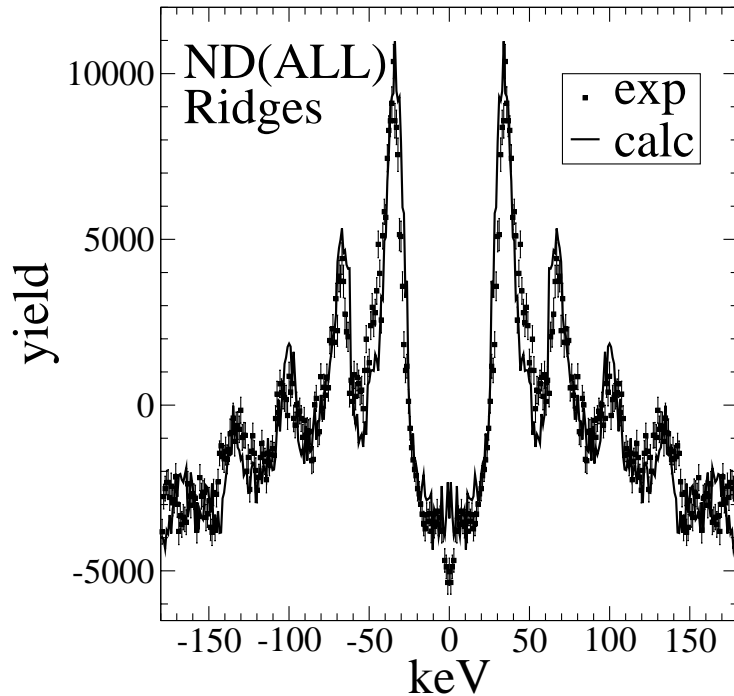


**Figure 3.** The ridges obtained when coincidence gates are placed on the same ND lines in  $^{152}\text{Dy}$  as in Fig. 2. The points with error bars are the data. The solid line is a calculation of the ridges. Most of the narrow ridge structure is from  $\gamma$  rays emitted while the nucleus is prolate superdeformed. Only the slowly changing underlying ridge structure is from  $\gamma$  rays emitted when the nucleus is normal deformed (mostly slightly oblate).

and SD states. The barrier penetration attenuation is large if the SD state is deep in the SD well, and near unity at the top of the barrier. On the other hand, if the nucleus is in a state in the ND well, the four calculated decay widths in the SD well are attenuated correspondingly. The subsequent decay path is selected in a Monte Carlo fashion from values of the eight decay widths. If a ND decay width is selected then the decay occurs in the ND well and visa versa.

For E2 transitions, first the wide or narrow component is selected. An additional Gaussian deviation around the mean energy (determined by the moment of inertia and the spin) is added, the width of which is based on the input rotational damping values:  $\Gamma_{wide}$  and  $\Gamma_{nar}$ . This is actually done before the final E2 decay widths are calculated, since the  $E^5$  term in the decay width formula will strongly favor E2 decays where the (mostly) wide component happens to add to the decay  $\gamma$ -ray energy, giving rise to an important extra cooling of the  $\gamma$  cascades.

In the simulations, the single  $\gamma$  rays of the cascades are binned, forming the QC spectra displayed in Figs. 1 and 2. For the ND (or more appropriately ALL) QC, Fig. 2, all  $\gamma$  cascades are used. For the SD QC, Fig. 1, only cascades trapped in the SD well, which happens about 2% of the time, are used.

The calculated  $\gamma$ - $\gamma$  coincidences in the cascades, are binned in 2D  $\gamma$ - $\gamma$  matrices after correcting for the experimental detector efficiency. The simulated 2D  $\gamma$ - $\gamma$  coincidence matrices have peaks and 'stripes' removed (although discrete peaks are not included in the model), and are core subtracted, *exactly* like the experimental data. Subsequently, the ridge spectra are produced by projecting cross-diagonally from the same  $\gamma$  energy region as for the experimental matrices. Figs. 3 and 4 presents the ridges obtained this way with the same selection of cascades as for the experimental QC spectra.

Work is in progress to measure the entry distribution. However, at the moment, a calculated entry distribution from a modified EvapOR code is used [24]. The  $\Gamma_{wide,nar}$  values, as well as the selected fraction of each, will depend on both spin and excitation energy. However, in this first attempt to calculate the QC and ridge spectra, constant values are used for simplicity in these demanding simulations.

## CONCLUSIONS AND FUTURE PROSPECTS

As can be seen in Figs. 1 to 4, the simulated spectra compare well with the data, especially considering the limitations of the simulations discussed above. The simulated spectra are shown with the best determined parameters, the most important of which are listed in Table 1. Ridges as narrow as the ones observed in Fig. 4 have also been observed in  $^{194}\text{Hg}$  [25]. At least four ridges are observed as well as a shallow valley in Fig. 4. The sharp ridges seen in Fig. 3 are

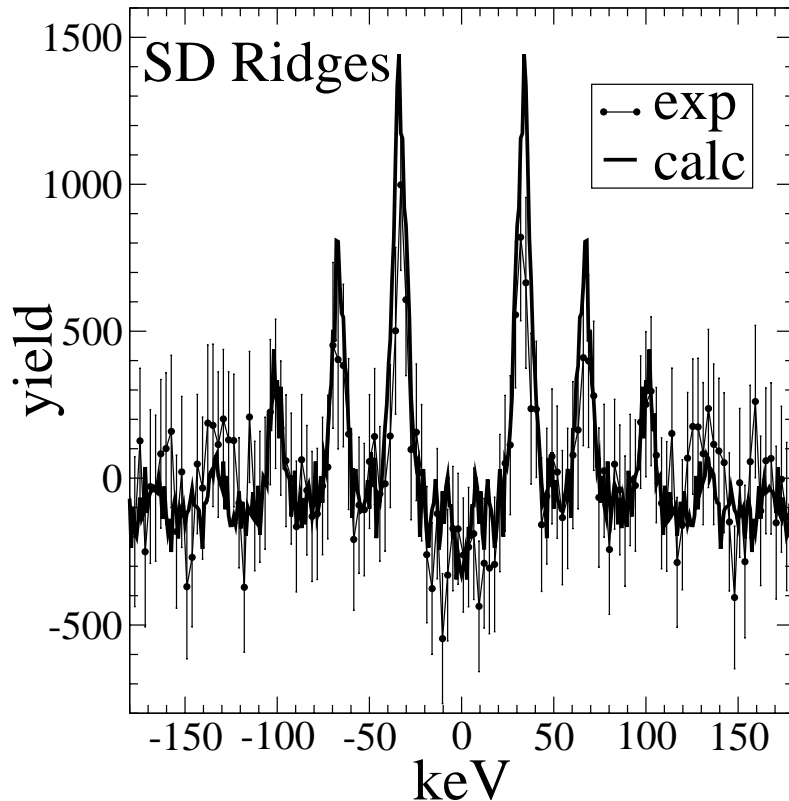


**Figure 4.** The ridges obtained when coincidence gates are placed on clean pairs of SD lines in  $^{152}\text{Dy}$ . At least four ridges can be seen. From the width of the narrow component of the ridge and the wide component, it has been possible to, for the first time, extract the rotational damping in the SD well of a nucleus:  $\Gamma_{nar} \sim 10$  keV and  $\Gamma_{wide} \sim 340$  keV. The solid line is a calculation of the ridges with these rotational damping widths.

from  $\gamma$  rays emitted while the nucleus is in the SD well, while the deeper valley is from the  $\gamma$ - $\gamma$  correlations in the ND well.

To improve the simulations, a dedicated experiment to measure the entry distribution for the reaction populating the  $^{152}\text{Dy}$  channel has been performed and the analysis is in progress. The next step will be to use spin and energy dependent  $\Gamma_{wid,nar}$  distributions both for the narrow and wide components, as well as variable fractions between them, from Ref. [12] to see if the measured ridges and QC spectra can be reproduced better. This will first be done in the ND well, subsequently in the SD well, where the theory in Ref. [12] may not be so robust. First exploratory attempts have shown that the  $\Gamma_{wide}$  values from Ref. [12] in the ND minimum works well (i.e., it improves the calculated ND QC spectrum significantly), but Ref. [12] underestimates the  $\Gamma_{wide}$  values in the SD well. However, it will take further Monte Carlo simulations and analysis to confirm this preliminary statement and there are also other calculations [26]. The calculations in Ref. [12] also agree well with the two different ND  $\Gamma_{wide}$  values that had to be used in the feeding at high spins, and decay-out at lower spins.

As can be seen in Fig. 1, the feeding and decay-out QC  $\gamma$  rays overlap significantly and they are reversed compared to the  $A \sim 190$  mass region. This analysis shows that in the  $A \sim 150$  mass region, it may be difficult to experimentally extract the decay-out QC and determine spin and excitation energy, as was done in the  $A \sim 190$  mass region [9].

In the feeding region, where the spin is high, there is quite clearly no pairing left. However, it was found that in order to reproduce the QC in Fig. 1 for the decay-out  $\gamma$  rays, somewhat larger pairing strength than indicated in Ref. [28] had to be applied, see Table 1. From the simulations, it is also found that  $\sim 20\%$  of all the  $\gamma$  rays in this reaction, at this beam energy, are emitted while the nucleus is SD – even though only  $\sim 2\%$  end up in the observed discrete SD bands. As a matter of fact, the ridges in Fig. 3 are so dominated by the  $\gamma$  rays emitted while the nucleus is in the SD well that the ridges associated with  $\gamma$  decays in the ND well are somewhat obscured. It is probably worthwhile to measure the ridges at a lower beam energy, where the nucleus will spend less time in the SD well, to determine the  $\Gamma_{wid,nar}$  values in the ND well with less interference and, thus, with better accuracy.

The analysis presented here is in progress and all results should be considered preliminary.

**TABLE 1.** Key parameters used in the Monte Carlo simulations presented in Figs. 1–4. The average static moment of inertia is denoted  $J^{(1)}$ . The extracted values of the rotational damping width  $\Gamma_{wide}$ , wide and narrow components, as well as the fraction of the narrow component that was selected, are shown. These values represent *average* values in the relevant spin and excitation energy regions. The values of the back-shift parameter in the level density formula [27] is denoted  $\Delta$ .  $\Gamma_{wide}$  and  $\Gamma_{nar}$ , which are FWHM measures, are related to  $\Gamma_{rot}$  and  $\Gamma_{\mu}$  in [15, 16] as shown.

parameter	ND well decay-out	ND well feed	SD well
$J^{(1)}$ MOI	$73\hbar^2/\text{MeV}$	$73\hbar^2/\text{MeV}$	$85\hbar^2/\text{MeV}$
$\Gamma_{nar} \sim 2\Gamma_{\mu}$		$\sim 24$ keV	$\sim 10$ keV
$\Gamma_{wide} \sim 2\Gamma_{rot}$	300 keV	610 keV	340 keV
narrow fraction	0 %	17 %	30 %
$\Delta$ back-shift	$\sim 1.5$ MeV	0 MeV	0 MeV

## ACKNOWLEDGMENTS

This work was supported in part by the U.S. Department of Energy, Office of Nuclear Physics, under Contract No. W-31-109-ENG-38 and DE-AC03-76SF00098, and the Danish Natural Science Foundation.

## REFERENCES

1. R. V. F. Janssens and T. L. Khoo, *Annu. Rev. Nucl. Part. Sci.* **41**, 321 (1991).
2. P. Nolan *et al.*, *J. Phys G* **11**, L17 (1985).
3. B. Nyako *et al.*, *Phys. Rev. Lett.* **52**, 507 (1984).
4. P. J. Twin *et al.*, *Phys. Rev. Lett.* **55**, 1380 (1985).
5. P. J. Twin *et al.*, *Phys. Rev. Lett.* **57**, 811 (1986).
6. T. Lauritsen *et al.*, *Phys. Rev. Lett.* **88**, 042501 (2002).
7. T. Lauritsen *et al.*, *Phys. Rev. Lett.* **89**, 282501 (2002).
8. I.-Y. Lee, *Nucl. Phys.* **A520**, 641c (1990).
9. T. Lauritsen *et al.*, *Phys. Rev. C* **62**, 044316 (2000).
10. R. Holzmann *et al.*, *Phys. Rev. Lett.* **62**, 520 (1989).
11. G. Leander *et al.*, *Phys. Rev. C* **25**, 2780 (1982).
12. B. Lauritzen *et al.*, *Nucl. Phys.* **A457**, 61 (1986).
13. M. Matsuo *et al.*, *Nucl. Phys.* **A557**, 211c (1993).
14. S. Leoni *et al.*, *Phys. Rev. Lett.* **96**, 4484–4487 (1996).
15. M. Matsuo *et al.*, *Phys. Lett.* **B465**, 1 (1999).
16. S. Leoni *et al.*, *Phys. Rev. Lett.* **93**, 022501 (2004).
17. S. Leoni *et al.*, *ibid.* (2004).
18. M. A. Deleplanque *et al.*, *ibid.* (2004).
19. B. Crowell *et al.*, *Nucl. Instrum. Methods* **A355**, 575 (1994).
20. D. C. Radford *et al.*, *Nucl. Instrum. Methods* **A258**, 111 (1987).
21. M. A. Bentley *et al.*, *J. Phys. G* **17**, 481 (1991).
22. M. P. Carpenter *et al.*, *Nucl. Instrum. Methods* **A353**, 234 (1994).
23. O. Andersen *et al.*, *Phys. Rev. Lett.* **43**, 687 (1979).
24. J. R. Beene *et al.*, *ftp.ornl.phy.ornl* (2004).
25. A. Lopez-Martens *et al.*, *Conference on Frontiers of Nuclear Structure*, Berkeley, CA, July 29-August 2, 2002, LBNL-50598 Abs., Book of Abstracts, p. 29 (2002).
26. K. Yoshida and M. Matsuo, *Nucl. Phys.* **A636**, 169 (1998).
27. A. Bohr and B. Mottelson, *Nuclear Structure Vol. 1*, Benjamin New York, 1969.
28. J. Dudek *et al.*, *Phys. Rev. C* **38**, 940 (1988).